ELSEVIER

Contents lists available at ScienceDirect

Combustion and Flame

journal homepage: www.elsevier.com/locate/combustflame



Experimental support for a new NO_x formation route via an HNNO intermediate



Joe Lee^a, Mark C. Barbet^a, Qinghui Meng^a, Rodger E. Cornell^{a,b}, Michael P. Burke^{a,c,d,*}

- ^a Department of Mechanical Engineering, Columbia University, New York, NY 10027, United States
- ^b US Army DEVCOM Armaments Center, Detonation Physics and Experimental Research Branch, Picatinny Arsenal, NJ 07806, United States
- ^c Department of Chemical Engineering, Columbia University, New York, NY 10027, United States
- ^d Data Science Institute, Columbia University, New York, NY 10027, United States

ARTICLE INFO

Article history: Received 6 August 2022 Revised 11 January 2023 Accepted 11 January 2023 Available online 21 February 2023

Keywords: NO_x formation Flame chemistry Kinetic modeling Nitrogen chemistry Jet-stirred reactor

ABSTRACT

Achieving minimal levels of nitrogen oxides (NO_x) during combustion is a major constraint in the design of advanced high-efficiency engines. NO_x can be formed during combustion of any fuel-including those without fuel-bound nitrogen-in air, where radicals can attack molecular nitrogen (N2) present in air to break the strong N-N bond to ultimately form NOx. Paramount to the goal of minimizing NOx formation is knowledge of the fundamental routes by which the strong N-N bond in N_2 can be broken. Historically, there have been four known routes for breaking the strong N-N bond in N_2 to ultimately form NO_x. We have recently posited that another route-mediated by an HNNO intermediate-may also play a role, particularly at the high pressures and low peak temperatures relevant to high-efficiency, low-NO_x engines. Our previous theoretical and modeling studies show HNNO to be a major product of the N_2O + H reaction at high pressures and low temperatures; once formed, HNNO is likely to react with radicals in barrierless reactions that would occur quickly and with high NO_x yields. In the present paper, we report measurements of H₂, O₂, H₂O, N₂O, NO, NO_x, and NH₃ in jet-stirred reactor experiments for an H₂/O₂/N₂O/NO/N₂/Ar mixture that specifically target HNNO pathways. Importantly, we observe significant formation of NO and NH3-both of which provide signatures of the HNNO mechanism that are not predicted by previous models without it. Flame simulations using a new sub-model describing pressuredependent formation and consumption of HNNO show these pathways to be among the most prominent formation routes at high pressures and low peak temperatures. However, exact quantification of the role of HNNO in NO_x formation and quantitative predictions of NO_x in general require more accurate rate constants for both HNNO pathways and mixture rules for pressure-dependent reactions.

© 2023 The Combustion Institute. Published by Elsevier Inc. All rights reserved.

1. Introduction

The formation of nitrogen oxides (NO_x) during combustion is a topic of long-standing and recent interest. Of considerable societal and engineering relevance, NO_x is an undesirable byproduct of combustion leading to smog and ground-level ozone with detrimental impacts on human and environmental health. Consequently, achieving minimal levels of NO_x to meet increasingly strict regulations is a major constraint in the design of advanced high-efficiency engines.

As summarized in the landmark review by Miller and Bowman [1] and the recent review of Glarborg et al. [2], NO_x can be formed during combustion of any fuel—including those without fuel-bound

E-mail address: mpburke@columbia.edu (M.P. Burke).

nitrogen—in air, where radicals can attack molecular nitrogen (N_2) present in air to break the strong N–N bond to ultimately form NO_x . The formation of NO_x during combustion in air is both kinetically limited and extraordinarily complex. Multiple formation routes—each with unique dependence on local, instantaneous thermodynamic conditions—contribute to NO_x formation at the high pressures and low peak temperatures of interest to advanced, low- NO_x engines [3,4]. Unsurprisingly, knowledge of the fundamental routes by which the strong N–N bond in N_2 can be broken is of paramount importance to the goal of minimizing NO_x formation—in terms of both qualitative understanding of how NO_x formation depends on thermodynamic conditions and quantitative predictions of NO_x formation, particularly under extrapolation.

Historically, there have been four known routes for breaking the strong N-N bond in N_2 to ultimately produce NO_X and other fixed nitrogen species [2]. In the so-called thermal mechanism proposed by Zeldovich [5], the N-N bond is broken via reactions of N_2 with

^{*} Corresponding author at: Department of Mechanical Engineering, Columbia University. New York, NY 10027. United States.

atomic oxygen

$$O + N_2 = NO + N \tag{R1}$$

to produce NO directly and indirectly through the subsequent reactions of N with O_2 and OH. Given the high activation energy of rate-limiting step (R1) to break the N–N bond in the Zeldovich/thermal mechanism, the Zeldovich mechanism is extremely sensitive to temperature. At sufficiently high temperatures, it is the dominant formation route for NO_x . However, at the lower peak temperatures of interest to advanced, single-digit NO_x engines, other routes become major contributors to NO_x formation [6].

In the "prompt" mechanism proposed by Fennimore [7], the N-N bond is broken via reactions of N_2 with CH_x radicals, notably CH. Contrary to the reaction originally postulated, the work of Moskaleva and Lin [8] has now established the reaction to be

$$CH + N_2 = NCN + H \tag{R2}$$

where NO_X is formed via subsequent reactions initiated by NCN. The Fennimore mechanism can be a significant major source of NO_X at richer conditions [1] where fuel-derived radicals are more prominent. Recent studies have indicated that the relative importance of this mechanism is diminished at higher pressures [4,9] in large part due to lower concentrations of CH at higher pressures [9].

In the NNH mechanism [10], the N-N bond is broken via reactions of an NNH intermediate formed from

$$H + N_2(+M) = NNH(+M) \tag{R3}$$

with atomic oxygen

$$NNH + O = NO + NH \tag{R4}$$

producing NO directly and indirectly via subsequent reactions of NH. Previous studies have found the NNH mechanism to be important across a wide range of equivalence ratios in premixed configurations [11] as well as non-premixed flames [12].

Finally, in the N_2O mechanism, the N-N bond is broken via reactions of an N_2O intermediate formed from

$$O + N_2(+M) = N_2O(+M)$$
 (R5)

with O or H

$$N_2O + O = NO + NO \tag{R6}$$

$$N_2O + H = NO + NH \tag{R7}$$

where subsequent reactions of NH produce additional NO_x . The N_2O mechanism, which is often called the "high-pressure" mechanism, is considered to be most significant at lean, high-pressure conditions where other mechanisms are suppressed and the rate constant for the pressure-dependent reaction (R5) is higher. In fact, computational studies have suggested that the N_2O mechanism is the dominant source of NO_x at the higher pressures and lower peak temperatures of interest to high-efficiency, low- NO_x engines [4].

We have recently posited [13] that another route—mediated by an HNNO intermediate—may also play a role, particularly at the high pressures and low peak temperatures relevant to high-efficiency, low-NO $_{\rm X}$ engines. For context, the N $_{\rm 2}$ O + H reaction (including (R7) and its competitive channels) is known to proceed via HNNO complexes [14–16], which can be stabilized at lower temperatures and higher pressures via the pressure-dependent reaction

$$H + N2O(+M) = HNNO(+M)$$
 (R8)

where HNNO is used here to collectively refer to t-HNNO, c-HNNO, and ONHN. (Note that, while (R4) also proceeds via HNNO complexes, the higher-energy complexes formed from NNH + O dissociate too rapidly to undergo much stabilization at combustion-relevant pressures.) Our theoretical calculations for an Ar bath gas

[13] indicate that stabilized HNNO is the dominant product of the H + N_2O reaction at temperatures below ~ 1300 K and favored over NO + NH below ~ 1600 K at 30 atm (a pressure relevant to many stationary gas turbine engines). The branching fraction to HNNO is likely even higher in the presence of stronger colliders like H_2O and CO_2 [17–19], whose mole fractions reach tens of percent in many combustion scenarios.

Our electronic structure calculations suggest that HNNO, once formed from (R8), reacts with radicals in barrierless reactions that would occur quickly and with high NO $_{\rm X}$ yields [13]. For example, our calculations (consistent with other studies [20–22]) suggest that H, OH, and O can add barrierlessly to HNNO to form complexes with submerged dissociation channels yielding NO $_{\rm X}$ and other fixed nitrogen species

$$HNNO + H = NO + NH_2 \tag{R9}$$

$$HNNO + OH = HNOH + NO$$
 (R10)

$$HNNO + O = HNO + NO \tag{R11}$$

where subsequent reactions of NH_2 , HNOH, and HNO can also yield additional NO_x . Consequently, based on the fact that this HNNO mechanism involves another pressure-dependent stabilization reaction beyond the N_2O mechanism, the HNNO mechanism might be expected to be increasingly favored relative to the N_2O mechanism at higher pressures and lower peak temperatures. Similarly, based on the fact that it does not involve carbon atoms, the HNNO mechanism may be especially relevant to NO_x formation during combustion of H_2 , a carbon-free renewable fuel of considerable recent interest where the Fennimore mechanism is inactive.

Yet, while HNNO has been considered as a species in some theoretical studies and in some kinetic models [23], pressure-dependent formation of HNNO is not considered in kinetic models [2,16,23–29] and HNNO has not been known to play a role in NO_X formation. Similarly, while theoretical calculations for $H+N_2O$ are in close agreement with experimental data at conditions where stabilization is prominent [16,30], we are not aware of previous validation datasets that are sensitive to the HNNO mechanism—despite the fact that our modeling studies find it to be among the dominant routes at the high pressures and low peak temperatures of interest to high-efficiency, low- NO_X engines [13].

Therefore, the objectives of the present paper are to experimentally verify the existence of the HNNO mechanism for NO_x formation, provide an assessment of an initial model describing pressure-dependent formation and consumption of HNNO, and use this HNNO sub-model to evaluate the role of the HNNO mechanism in NO_x formation in flames at some representative conditions. Herein, we report species measurements from jet-stirred reactor experiments using an H₂/O₂/N₂O/NO/N₂/Ar reactant mixture specifically chosen to accentuate the above-mentioned HNNO pathways and therefore discriminate their existence. Notably, the formation of both NO and NH3 during reaction of this mixture at low temperatures provide signatures of the HNNO mechanism that are captured using our HNNO sub-model but not predicted by previous models without it. Finally, we present flame simulations using this new sub-model describing pressure-dependent formation and consumption of HNNO that reveal these pathways to be among the most prominent formation routes at high pressures and low peak temperatures.

2. Experimental methods

Experiments to accentuate the pathways involved in the HNNO mechanism were conducted at the conditions listed in Table 1 over an intermediate temperature range using the jet-stirred reactor

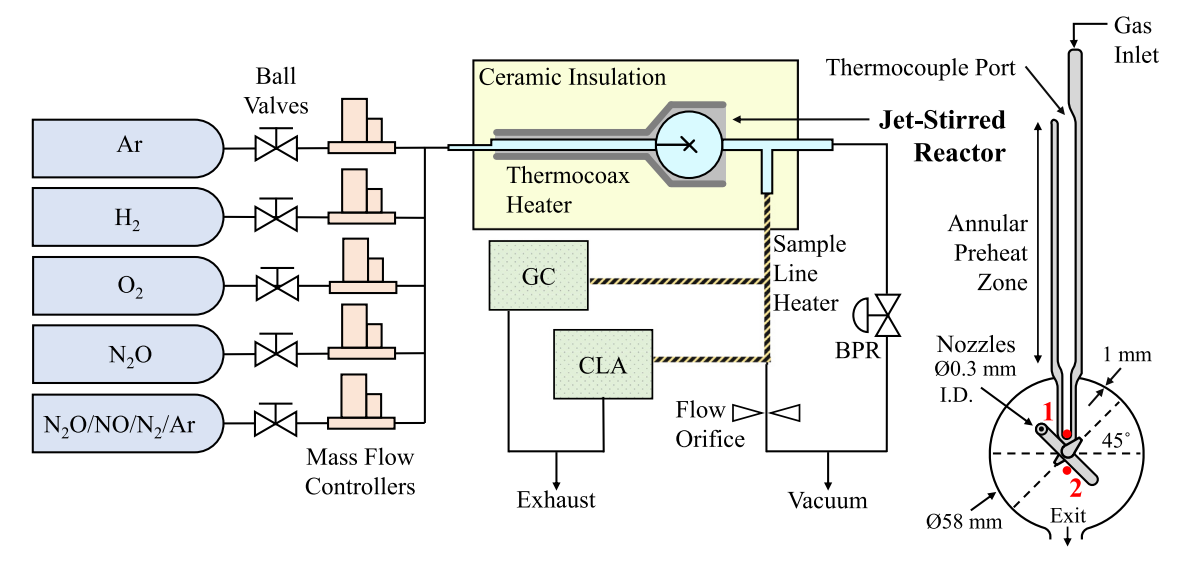


Fig. 1. A simplified schematic of the atmospheric-pressure jet-stirred reactor system used for this study.

 Table 1

 Experimental conditions with estimated uncertainties.

•	
Mixture composition	5000 ppm N_2O ($\pm 2\%$) 4000 ppm H_2 ($\pm 3\%$) 800 ppm O_2 ($\pm 2\%$) 37.5 ppm NO ($\pm 2\%$) 244.5 ppm N_2 ($\pm 2\%$) balance Ar
Residence time	1.2 s (±5%)
Pressure	1.02 atm (±1%)
Temperature	650-1180 K (±1%)

(JSR) facility (Fig. 1) used in previous studies of nitrogen kinetics by Cornell et al. [31,32]. Of note, this facility features a flow delivery system capable of preparing diverse multi-component reactant mixtures to sensitize the exact kinetics of interest (such as in the present experiments chosen by an ad hoc experimental design and for planned experiments chosen by optimal experimental design [33]) and several rapid-response inline species diagnostics for high-throughput and/or semi-automated operation to maximize the information generation rate [34]. The experimental conditions in Table 1 were chosen based on computational screening of experimental conditions and observables with the goal of clearly distinguishing between models with and without HNNO pathways in a manner minimally affected by thermal boundary conditions (as assessed by comparing isothermal JSR and adiabatic JSR simulations), extent of mixedness (as assessed by comparing perfectly stirred reactor and plug flow reactor simulations), and uncertainties in experimental conditions and rate constants for known reactions (as shown below).

Reactant mixture preparation and flow control was achieved through a bank of Bronkhorst EL-FLOW Prestige thermal mass flow controllers (MFCs), which flow each gas into the mixing manifold before entering the reactor. To reach the experimental conditions listed in Table 1, a certified gas mixture of $N_2O/NO/N_2/Ar$ supplied by Airgas was supplemented by research grade (99.999% purity) tanks of N_2O , O_2 , H_2 , and Ar to give total volumetric flow rates between 0.988 and 1.79 L/min (with a $\pm 2\%$ uncertainty). These volumetric flow rates were chosen in order to yield a fixed residence time of 1.2 s across the experimental temperature range (650–1180 K). The uncertainties listed in Table 1 for the mole fraction

of each component in the reactant mixture are based on specified uncertainties of $\pm 0.5\%$ of the reading plus $\pm 0.1\%$ of the full scale for each MFC.

The fused quartz JSR used in the present work was constructed based on the design of Herbinet et al. [35,36], which conforms to the design rules introduced by Villermaux and others [37,38]. This particular design has been found to closely resemble the behavior of a perfectly stirred reactor under its designed conditions [39,40] and has been widely used in many previous kinetic studies [31,32,35,36,41,42]. Immediately prior to entry into the spherical reactor, the gas flows through an annular preheating zone (whose volume is less than 10% of the JSR volume) with low residence time and large surface area to heat the gas mixture rapidly and therefore maintain thermal homogeneity in the reactor [43]. The gas then flows into the reactor via four ~ 0.3 mm nozzles in a crossed configuration angled 45° from the equatorial plane to promote turbulent mixing and large recycling rates and, therefore, promote homogeneity within the reactor. Our measurements [31] of the reactor volume via water displacement found an internal reactor volume of 82 ± 2 cm³; uncertainty in this volume measurement combined with uncertainties in the gas flow rates lead to estimated uncertainties in the nominal residence times in the ISR of approximately $\pm 5\%$.

The temperature in the spherical reactor is controlled by a Thermocoax resistive heating element wrapped around the reactor and preheating zone and powered by a Digi-Sense temperature controller. The temperature is monitored using two Omega K-type thermocouple probes (whose locations are indicated as red dots in Fig. 1) rated for $\leq \pm 1.5$ K noise, $\leq \pm 1.5$ K deviation from linearity, and $\leq \pm 2.8$ K calibration drift. Thermocouple '1' is located directly inside the nozzle array via an inner concentric access port within the annular preheat zone. Thermocouple '2' is encased in a sealed 2-mm-diameter quartz tube inserted through the outlet with the tip positioned near the center of the reactor for the present experiments, though it can be translated radially to measure temperature homogeneity. Radial translation of Thermocouple '2' (along with comparisons against readings from Thermcouple '1') in Ar at nominal setpoint temperatures ranging from 700 to 1180 K have indicated spatial temperature uniformity within ± 5 K [31].

The reactor pressure is maintained with an Equilibar domeloaded back pressure regulator in the exhaust line from the reactor using the pressure signal provided by an Omega digital pressure gauge located just downstream of the reactor. The pressure used in the experiments is maintained at 15.00 psia. Based on the uncertainties in the pressure regulator and measured variability in flow control [31], the estimated uncertainty in this pressure is $\leq \pm 1\%$ in the present experiments.

The diagnostics used in the experiments draw sample gas from the reactor outflow via silica-coated stainless-steel pipes maintained at a temperature around 385 K using a secondary "sample line heater" to ensure all components of the reacted gas mixture remain in a vapor phase. In the present study, two diagnostics draw from this sample line to measure species mole fractions for each experimental condition.

Measurements of H₂, O₂, N₂O, and H₂O are provided by an Inficon Micro-GC Fusion gas analyzer (GC) using thermal conductivity detectors on an Rt-Molsieve 5 Å column for H2 and O2 and an Rt-Q-Bond column for H_2O and N_2O . Measurements of NO, NO_x , and NH₃ are provided by an Eco Physics AG nCLD-844 CMh chemiluminescence analyzer (CLA). Specifically, the CLA contains two independent cells that can each measure up to 500 ppm of NO. In addition to measuring NO directly (without the use of a converter), the first cell (A) also contains an NO_x converter that can convert up to 10 ppm of NO₂ into NO to give a measure of total NO_x. The second cell (B) also contains a converter to convert NO2 and amines to NO to give a measure of total NO_x-amines (where NH₃ would be the only significant amine here). When both converters are in operation, the device can provide a measure of NH₃ from the difference in the signals provided by cells A and B. Separate tests using mixtures of NO2 and NH3 in Ar prepared using the MFCs indicated that the conversion efficiency of the NO_x converter is nearly \sim 100% while the conversion efficiency of the NO $_{x}$ -amine converter is $\sim 92\%$.

Jet-stirred reactor experiments were performed in two separate runs, which were conducted 15 months apart—during which time the CLA was serviced and cleaned and one of the pumps from the GC was replaced. In each experimental run, species mole fractions were measured at each reactor temperature set point ranging from 650 to 1180 K. Each measurement was taken for approximately 10 min, allowing all exposed surfaces in the system to adsorb NH₃ until equilibrium is reached and mole fractions remain stable [44–46]. After each measurement, the CLA was flushed with pure Ar and re-calibrated using certified standard gas mixtures to minimize NH₃ exposure and calibration drift.

In the first experimental run, the mole fractions of N2O, H2, H₂O, O₂, and NO were measured. In the second experimental run, the mole fractions of N2O, H2, H2O, NO, NOx, and NH3 were measured. In each set of experimental runs, multi-point GC calibrations (over mole-fraction ranges encompassing the full range observed experimentally) were performed using mixtures of each species with varied mole fractions in Ar prepared by the MFCs for all species except for H₂O. For H₂O, during the first experimental run, multi-point GC calibrations were performed by flowing varied H₂/O₂/Ar mixtures into the heated JSR at temperatures where complete conversion of H₂ and O₂ to H₂O was observed. For the second experimental run, the initial multi-point calibration for H₂O was simply scaled to match the high-temperature plateau measured in the first experimental run. (Despite the indirect nature of this calibration procedure, the high-temperature plateau values for H₂O are essentially perfectly consistent with the amount predicted under complete conversion of H₂ to H₂O in the H₂/O₂/N₂O/NO/N₂/Ar experiments—as shown in Figs. 2 and 3.) As indicated in Figs. S2 and S3 of the Supplementary Material, hydrogen balances of \sim 95-100% and oxygen balances of \sim 90–100% were obtained across the experimental conditions (with the lowest oxygen balances corresponding to conditions where O2 was below the minimum measurement threshold). While not calibrated in the present experiments, the growth of N2 signals on the Rt-Molsieve 5 Å column (shown in Figs. S4 and S5) mirrored the fall of N₂O with increasing

Table 2 Measurement uncertainties for the gas chromatograph (GC).

Observable	N ₂ O	H ₂	H ₂ O	02
Calibration	±1-4%	±1-8%	±2-12%	±1-2%
Noise (1 σ)	±0.2-3%	$\pm 0.810\%$	±0.6-11%	±10-18%
Minimum	50 ppm	100 ppm	200 ppm	20 ppm

 Table 3

 Measurement uncertainties for the chemiluminescence analyzer (CLA).

Observable	NO	NO_x	NH ₃
Calibration	±2%	±2%	±2%
Drift	±2%	±1%	±2%
Linearity	±1%	±1%	$\pm 1\%$
Noise (1 σ)	±0.05-0.9%	±0.03-0.8%	±0.08-2%
Minimum	25 ppb	25 ppb	25 ppb

temperatures (consistent with model predictions indicating that N_2 is the main other N-containing species). Similar to Cornell et al. [31,32], sources of uncertainty for each species measured during this study are compiled in Tables 2 and 3; these uncertainties are combined to produce the error bars accompanying the experimental measurements in the figures below.

3. Simulation methods

Kinetic simulations were performed in Cantera 2.5.1 [47] using a variety of kinetic models. Simulations were performed using 9 kinetic models from the literature describing H/N/O kinetics: Glarborg et al. [2], Han et al. [23], Shrestha et al. [24], Stagni et al. [26], Otomo et al. [27], Zhang et al. [25], Lamoureux et al. [29], Klippenstein et al. [16], and GRI 3.0 Mech [28].

Simulations were also performed using variants of the model of Glarborg et al. [2] where the kinetics of HNNO isomers (t-HNNO, c-HNNO, ONHN) [13] were added. The HNNO sub-models for pressure-dependent formation and consumption of HNNO are all based on Meng et al. [13], where rate constants for all phenomenological reactions on the H + N $_2$ O PES [16], NH $_2$ + NO $_2$ PES (including OH addition to HNNO at the N site adjacent to O) [48], and HNNO + O $_2$ PES [13] were obtained from RRKM/ME calculations [13]. Due to the importance of third-body efficiencies in flame simulations [49,50], for the three most important pressure-dependent reactions within this set

$$H + N2O(+M) = t-HNNO(+M)$$
 (R12)

$$H + N2O(+M) = c-HNNO(+M)$$
 (R13)

$$t-HNNO(+M) = c-HNNO(+M)$$
 (R14)

the rate constants were accompanied by third-body efficiencies for H_2 , O_2 , N_2 , and H_2O using values assumed to be the same as those for $H + O_2$ (+M) from Burke et al. [51], which are also consistent with recent studies [17–19]. A proper treatment of the mixture composition dependence of rate constants in combustion simulations would require implementation of recently developed and validated reduced-pressure mixture rules [52–56], which are not yet available in any combustion codes. As an interim solution, the rate constants for (R12), (R13), and (R14) were expressed in Troe format with third-body efficiencies—an overall representation that is implemented in many combustion codes (including Cantera used

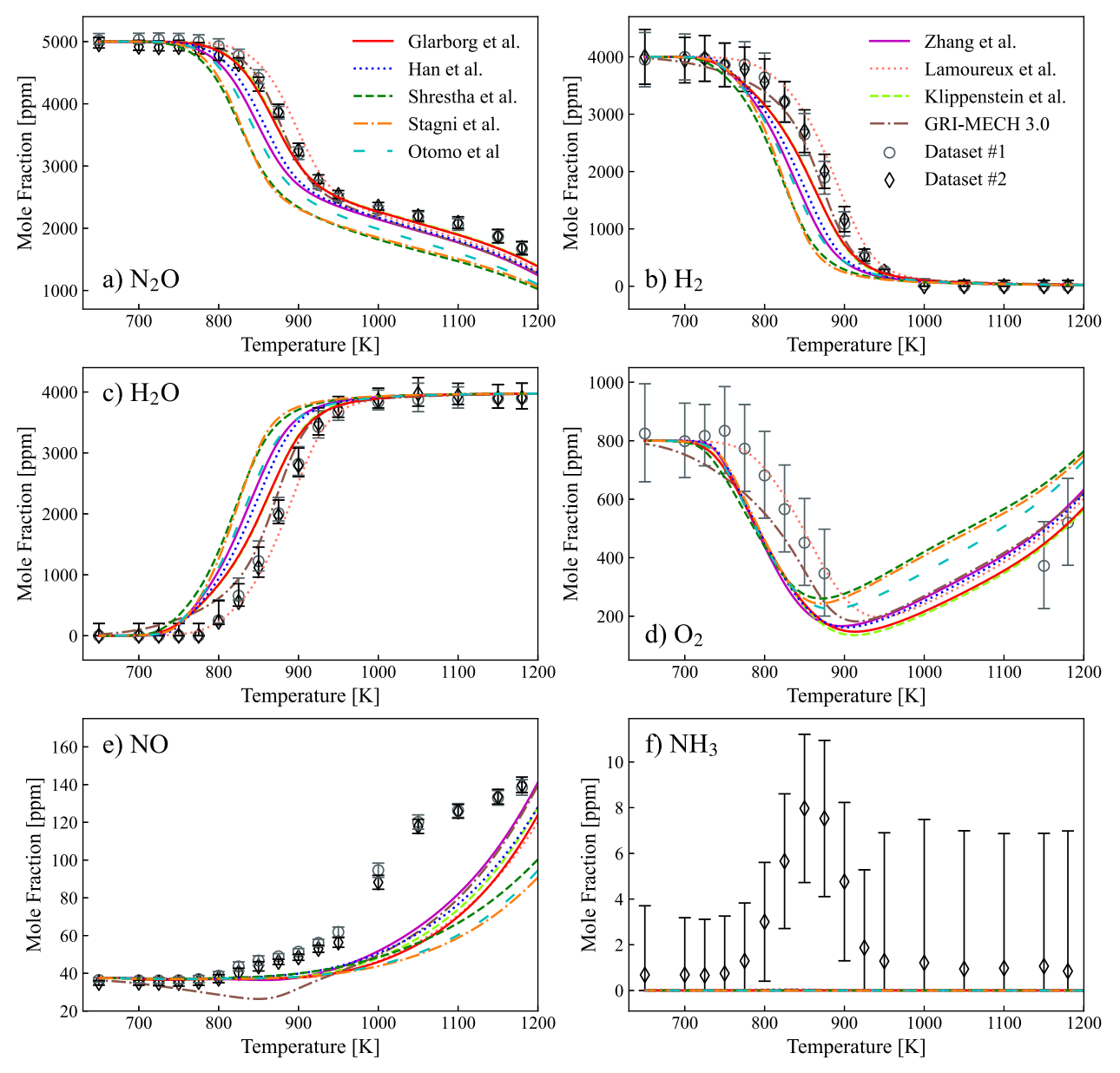


Fig. 2. Species mole fraction measurements and predictions using previous kinetic models [2,16,23-29] at the experimental conditions of Table 1.

here) using a mixture rule that is similar to our linear reduced-pressure mixture rule [52,54] but is much more limited in its capabilities. For example, this presently implemented mixture rule assumes (falsely) that third-body efficiencies are independent of temperature and pressure and, more importantly here, the Troe formula cannot provide even a qualitatively accurate representation of pressure dependence for multi-well/multi-channel reactions such as (R12)–(R14). While the rate constants for (R12)–(R14) can fortuitously be fitted using a Troe formula over pressures from 0.001 to 1000 atm (as is used in the HNNO sub-model), the lowand high-pressure limits in the fit are not meant to correspond to the actual limits and the representation is not meant for extrapolation.

The rate constants for all other HNNO + H, OH, and O reactions (except for those resulting from OH addition to the N site adjacent to O discussed above) were estimated based on preliminary electronic structure theory calculations which suggest that H, OH, and O can all add without intrinsic energy barriers and form the

products indicated in (R9), (R10), and (R11) as well as

$$HNNO + H = H + N_2 + OH \tag{R15}$$

$$HNNO + H = N_2 + H_2O \tag{R16}$$

$$HNNO + OH = N_2O + H_2O \tag{R17}$$

$$HNNO + O = N_2O + OH \tag{R18}$$

Specifically, the rate constants for HNNO + H (R9), (R15), (R16) were assigned values based on preliminary theoretical kinetics calculations near 1000 K and the rate constants for HNNO + OH at sites other than the N adjacent to O (R10), (R17) and for HNNO + O (R11), (R18) were assigned values near the collision limit.

For the purposes of comparison with the present jet-stirred reactor (JSR) experiments, isothermal, isobaric, perfectly stirred reac-

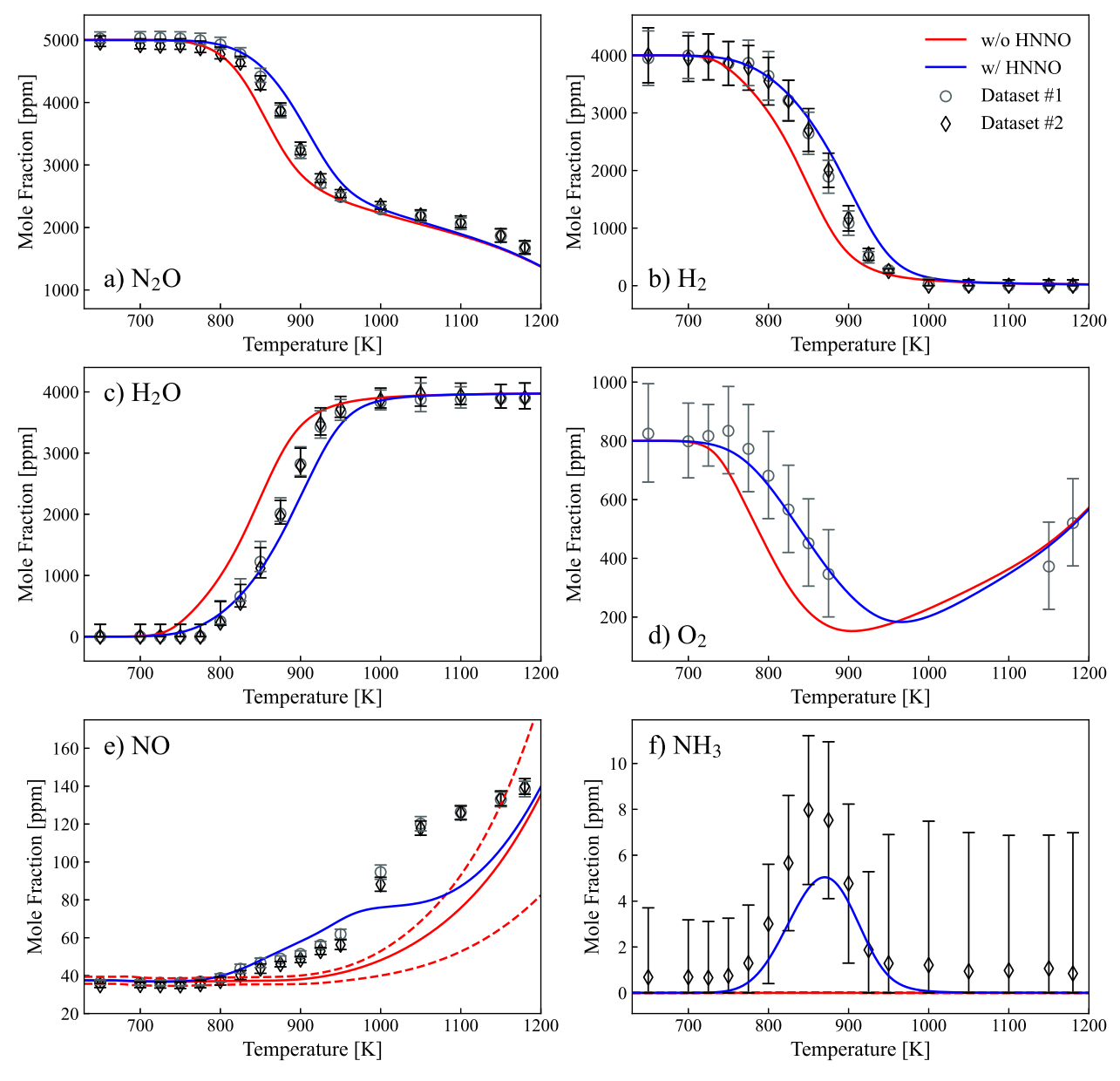


Fig. 3. Species mole fraction measurements and predictions using kinetic models with and without HNNO kinetics at the experimental conditions of Table 1. Prediction uncertainties for NO and NH₃ due to uncertainties in kinetic and physical model parameters are shown in the dashed lines for the model without HNNO kinetics.

tor (PSR) simulations were performed. For the purposes of evaluating the role of the HNNO mechanism in NO_x formation in flames, freely propagating premixed planar flame simulations were performed for H_2 /air and $H_2/O_2/N_2$ mixtures of varied equivalence ratios. To illustrate the influence of different aspects of the HNNO kinetic submodel on the flame predictions, simulations were also performed using model variants that employ different parameters as described below.

For the uncertainty-quantified model predictions shown in Fig. 3 below, which were calculated using our MultiScale Informatics package [34,58,57,59], the uncertainties include both uncertainties in rate constants using the recent uncertainty compilation from Cornell et al. [32] and uncertainties in physical model parameters [34] (reactant mole fractions, residence times, pressures, and temperatures) describing the experiments using the values in Table 1. (Inverse uncertainty quantification was not performed here using the present dataset or other datasets, so the uncertainties shown below correspond to the prior rather than posterior

distributions.) Uncertainties in each parameter were propagated into the model predictions for each species at each experimental condition using the sensitivity coefficients evaluated by Cantera [47].

4. Results and discussion

4.1. Experimental results and associated modeling analyses

Species measurements from the present jet-stirred reactor experiments are shown in Figs. 2 and 3. The two datasets for the species measured in both experimental runs (N_2O , H_2 , H_2O , and NO) are in very close agreement (and generally within experimental error bars), which suggests a high level of repeatability—especially when considering the long duration between the two experiments and changes to the diagnostics devices.

The measured mole fractions of all species show an onset of reactivity around ~ 800 K. At temperatures above ~ 1000 K, the

measured mole fraction of H_2 approaches zero and the mole fraction of H_2O likewise reaches a plateau. Over the whole temperature range, the N_2O mole fraction monotonically decreases with temperature though exhibits a less pronounced temperature dependence above ~ 1000 K where H_2 is completely depleted in the reactor. The O_2 mole fraction decreases with temperature at lower temperatures where H_2 is still substantively present but increases with higher temperatures where H_2 is essentially depleted and the oxygen liberated from N_2O consumption forms no additional H_2O (the other major species containing oxygen).

Notably, significant amounts of NO, NO_x, and NH₃ are also observed at temperatures as low as ~ 800 K. As shown in Fig. S1 of the Supplementary Material, the mole fractions of NO and NO_x, which both rise monotonically with temperature, are essentially indistinguishable from each other within experimental uncertainties—indicating that nearly all of the NO_x signal is attributable to NO (with negligible contributions from NO₂). While the measured mole fraction of NH₃ is negligible below \sim 800 K and above \sim 1000 K, it notably reaches clearly detectable amounts, peaking around ~ 850 K where the measured amount of NH₃ formed is comparable to the measured amount of NO formed.

As shown in Fig. 2, for N_2O , H_2 , H_2O , and O_2 , while predictions using many highly validated and widely used kinetic models [2,16,23–29] exhibit some differences in the predicted onset temperature for reactivity, they all generally reproduce the qualitative features of the temperature-dependent reactivity. However, for NO_x , and NH_3 , none of the models capture the observed behavior. All models predict negligible amounts of NO_x at lower temperatures (below $\sim 950~\rm K$) and negligible amounts of NH_3 at all temperatures.

In fact, as indicated by uncertainty-quantified model predictions without the HNNO mechanism displayed as red dashed lines in Fig. 3, uncertainties in conventional NO_{X} formation pathways, all other reactions, and physical model parameters [34] are insufficient to explain the experimental observations. Specifically, the dashed lines indicate the prediction uncertainties stemming from uncertainties in rate constants for all reactions in the kinetic model and uncertainties in the reactant mixture composition, residence time, reactor temperature, and reactor pressure. The measured NO and NH3 mole fractions greatly exceed these uncertainty bounds (which are meant to represent two standard deviations).

On the other hand, the model that includes HNNO pathways predicts significant NO and NH3 formation at these low temperatures (~800-950 K) where models without HNNO do not. In fact, model predictions including HNNO pathways based on our current estimates agree reasonably well with the experimental measurements for all species, including NO and NH3 at low temperatures. It should, of course, still be noted that there are some quantitative differences in model predictions (notably NO at higher temperatures and NH₃) that appear to be attributable to uncertainties in several reactions (both within the HNNO sub-model and others) and, particularly at higher temperatures, the physical model for the experiments. In spite of such uncertainties, the model with HNNO kinetics explains the observed formation of NO and NH₃ near $\sim 800\text{--}950~\text{K}$ in a way that conventional NO_x mechanisms do not. Altogether, the discussion above indicates that the present measurements provide strong experimental support for the NO_x formation route via HNNO.

To further elucidate the controlling kinetics that explain the observations, rate of production analyses for the key species were performed. Similarly, the net rates of reactions that involve a change in the maximum number of N atoms in a single species between the reactants and the products, which indicates a breaking of the N–N bond across the reaction, were also calculated. The discussion below focuses on the controlling kinetics at low tem-

peratures (~ 800 –950 K) where the four conventional NO $_{x}$ mechanisms are unable to explain the observed formation of NO and NH $_{2}$.

As indicated by Fig. 4, the reaction of N₂O with H

$$H + N_2O = N_2 + OH$$
 (R19)

to produce N_2 and OH and the reaction of OH with H_2

$$OH + H_2 = H_2O + H$$
 (R20)

to produce H_2O and H serve to explain most of the N_2O consumption, H_2 consumption, and H_2O formation and are the predominant contributors to the consumption of the key radicals H and OH. While not the main consumption route for H, the reactions of H with O_2

$$H + O_2 = OH + O$$
 (R21)

$$H + O_2(+M) = HO_2(+M)$$
 (R22)

are the primary consumption routes for O_2 and generate OH and O, which both react primarily with H_2 , or HO_2 , which mostly reacts with NO

$$HO_2 + NO = OH + NO_2 \tag{R23}$$

to form OH and NO2, which in turn mostly reacts with H

$$H + NO_2 = OH + NO \tag{R24}$$

to form OH—all of which also impact the radical pool at these conditions. (R23) and (R24) are also the primary production and consumption routes, respectively, for NO_2 and are of roughly equal magnitude, suggestive of NO_2 being in quasi-steady state (at very low mole fractions according to Fig. S1).

For NO and NH₃, a much larger number of reactions contribute substantively to their production and consumption, many of which simply interconvert fixed nitrogen species (e.g., NO, NO₂, HNO, and HONO; and NH₂ and NH₃). In that regard, the rates of reactions that involve a change in the maximum number of N atoms in a single species from the reactants to products provide a clearer indication of the reactions that break the N–N bond to initiate NO and NH₃ formation and/or form the N–N bond to return fixed nitrogen to N₂. For example, Fig. 4 also shows the values of

$$\omega_k^{\Delta n_N} = \omega_k (n_N' - n_N'')$$

for each reaction, k, where ω_k is the rate of reaction k, n_N' is the maximum number of N atoms in any single species in the reactants, and n_N'' is the maximum number of N atoms in any singles species in the products. In the present H/N/O kinetic models (where all species with more than 1 N atom have an N-N bond and all others do not), non-zero values for this quantity correspond to the rates of each reaction that results in the N-N bond being broken or formed. (However, in C/H/N/O systems, non-zero values for reactions of NCN, which has 2 N atoms but no N-N bond, would not correspond to N-N bond breaking, for example.) The results shown in Fig. 4 indicate that the primary reactions responsible for breaking the N-N bond at low temperatures (\sim 800–950 K) involve reactions of HNNO (predominantly t-HNNO) with H, OH, and O where each produce NO along with NH₂, HNOH, and HNO as co-products ((R9), (R10), and (R11) respectively).

Under the present conditions, where both NO and $\rm H_2$ are present in the reactant mixture, $\rm NH_2$ reacts with NO

$$NH_2 + NO = H_2O + N_2$$
 (R25)

$$NH_2 + NO = NNH + OH \tag{R26}$$

to return fixed nitrogen to N_2 (via rapid NNH decomposition to H + N_2 in the case of (R26)) or with either H_2 or H

$$NH_2 + H_2 = NH_3 + H$$
 (R27)

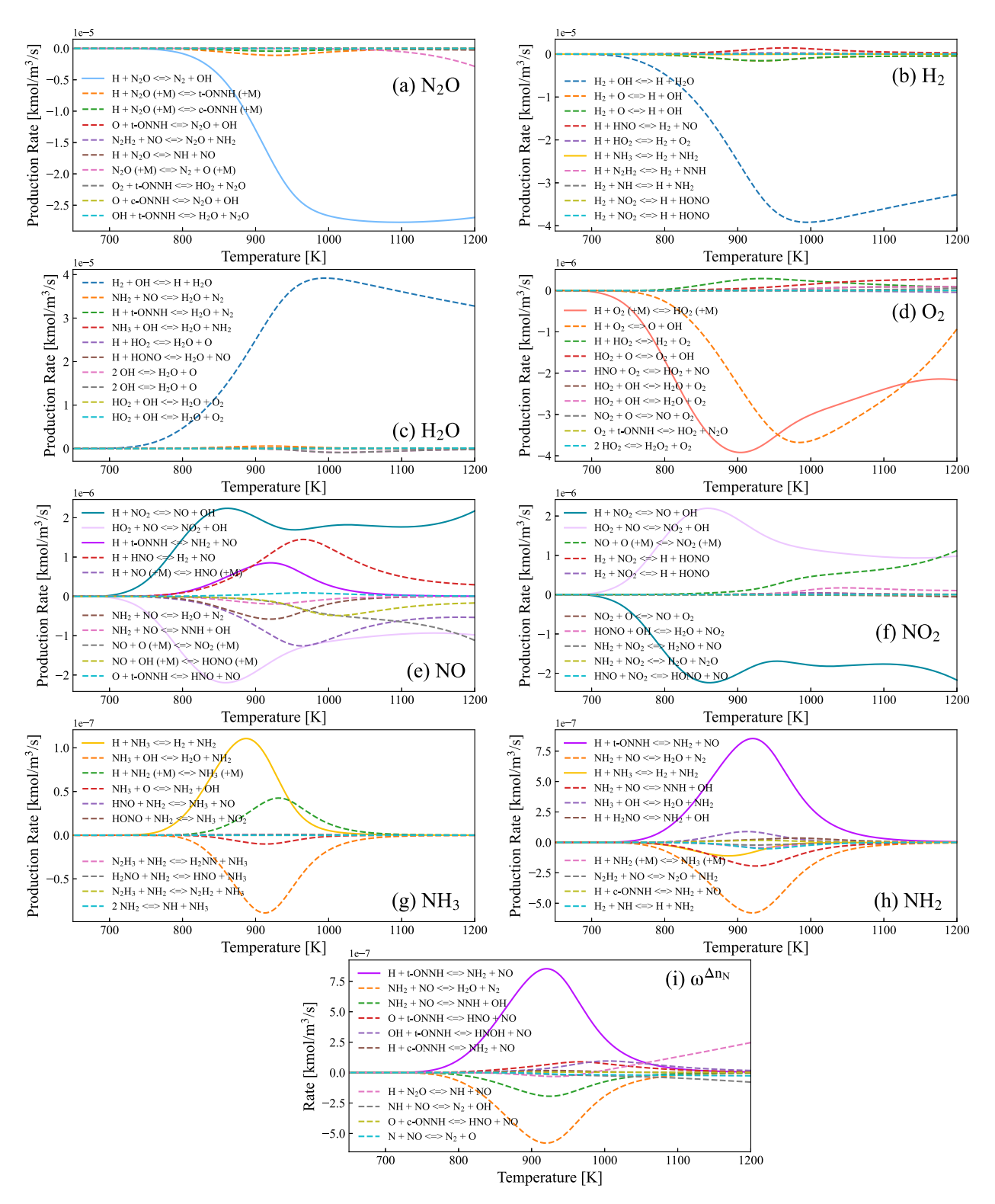


Fig. 4. Rates of production for N_2O , H_2 , H_2O , O_2 , NO, NO_2 , NH_3 , and NH_2 and net rates of reactions that involve a change in the maximum number of N atoms in any single species between the reactants and products (see text) using the model with HNNO kinetics at the conditions of the present experiments.

$$NH_2 + H(+M) = NH_3(+M)$$
 (R28)

to produce NH_3 . (At this point, it is worth noting that flame simulations indicate that the ultimate fate of NH_2 in lean and stoichiometric flames is additional NO rather than NH_3 .)

Therefore, the appearance of both NO and NH $_3$ in both the experiments and model predictions with HNNO pathways are consistent with the HNNO mechanism and cannot be explained via conventional NO $_x$ formation mechanisms. In fact, the detection of NH $_3$ near $\sim 800-950$ K is a clear signature of (R9) in particular.

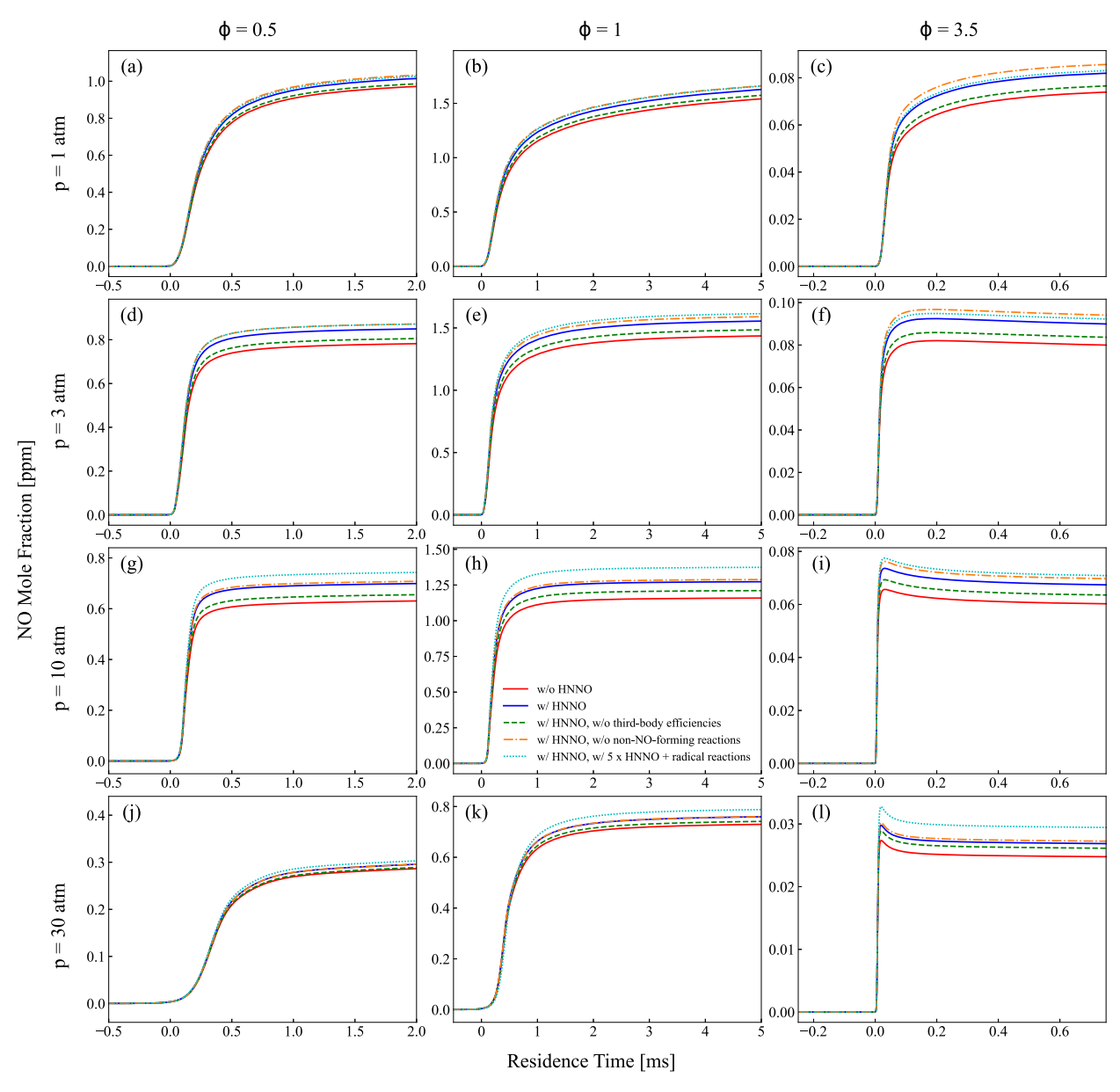


Fig. 5. Predicted NO mole fractions in freely propagating premixed $H_2/O_2/N_2$ flames for various pressures and equivalence ratios (that yield flame temperatures near \sim 1650 K). For equivalence ratios, ϕ , of 0.5 and 3.5, the N_2/O_2 mole fraction ratio is 3.76 (characteristic of air); for equivalence ratio, ϕ , of 1.0, the N_2/O_2 mole fraction ratio is 8.5 (to yield the same flame temperature as the lean and rich cases).

4.2. Implications for NO production in flames

To understand the role of the HNNO mechanism in NO_x formation from non-nitrogenous fuels in flames (a common combustion mode in many engines), freely propagating premixed flame simulations were performed for $H_2/O_2/N_2$ mixtures across varied pressures and equivalence ratios yielding flame temperatures near $\sim 1650~K$, where the Zeldovich mechanism is suppressed. Simulations were performed for various models to illustrate the role of HNNO in NO_x formation as well as the salient features of the HNNO pathways and impact of uncertainties in various aspects of the kinetic treatment. In addition to the model with HNNO kinetics from Meng et al. [13], variations of this model are also shown that exclude third-body efficiencies for $H + N_2O$ (to illustrate the influence of collider-specific rate constants and mixture rules), that exclude estimated HNNO + radical reactions to non-NO-forming products (R15), (R16), (R17), (R18) (to illustrate the in-

fluence of branching ratios for HNNO + radical reactions), and that have five times higher rate constants for all estimated HNNO + radical reactions (to illustrate the influence of total rate constants for HNNO + radical reactions). Predicted NO mole fractions from these simulations are displayed in Fig. 5 as a function of transformed distance: the "flame residence time", $\tau = d/s_b$, equal to the distance, d, divided by the burned gas flame speed, s_b (similar to elsewhere [60]).

As depicted in Fig. 5, model predictions that include HNNO kinetics yield appreciably higher NO mole fractions than those without HNNO kinetics for all equivalence ratios. Correspondingly, inspection of $\omega_k^{\Delta n_N}$ throughout the flame shown in Fig. 6 reveals that HNNO pathways are among the primary contributors to N–N bond breaking for all equivalence ratios, with significant contributions from HNNO + OH, O, and H at lean and stoichiometric conditions and from HNNO + H exclusively at very rich conditions. In fact, at very rich conditions, the HNNO mechanism appears to

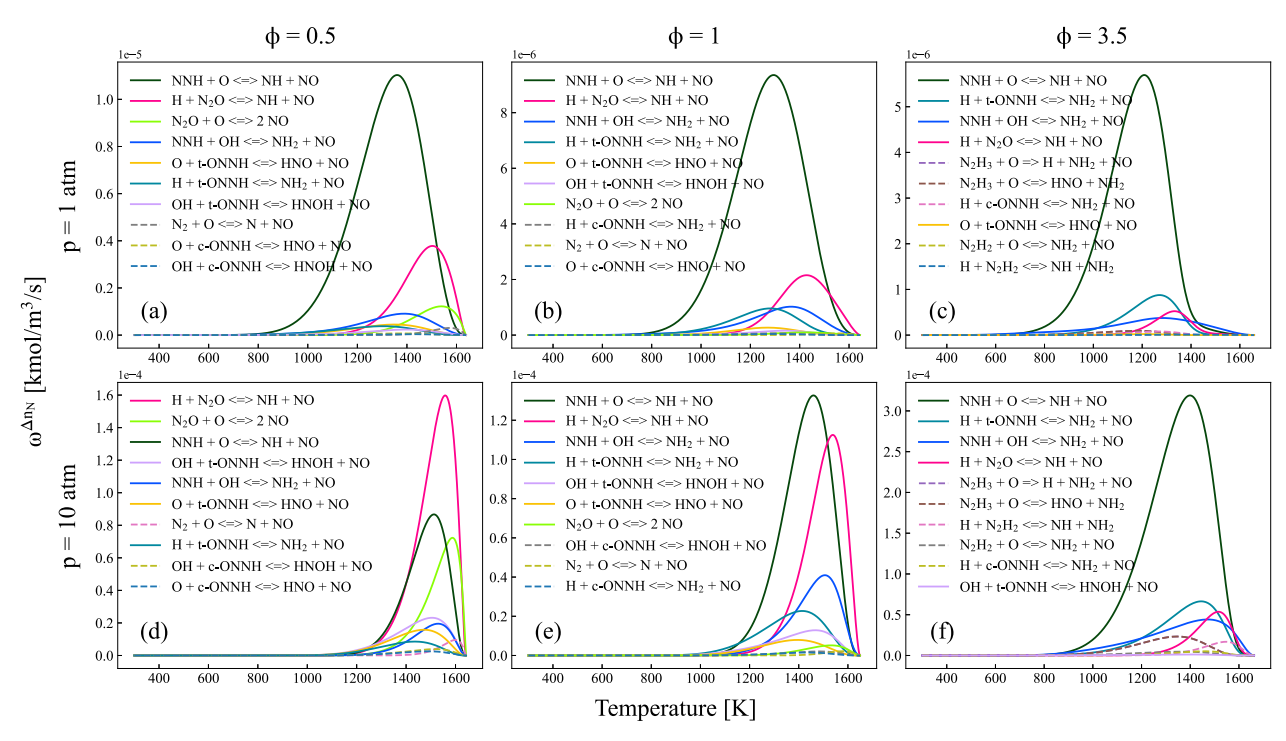


Fig. 6. Net rates of reactions that involve a change in the maximum number of N atoms in any single species between the reactants and products (see text) using the model with HNNO kinetics in the flames shown in Fig. 5.

be favored over the N_2O mechanism. While the NNH mechanism appears dominant for lean and stoichiometric conditions at low pressures and very rich conditions at all pressures, the N_2O and HNNO mechanisms (which both involve pressure-dependent reactions) become more prominent at higher pressures. Given the relevance of lean, high-pressure flames to practical engine conditions, additional analyses were performed to understand the relative roles of the N_2O and HNNO mechanisms. As shown in Fig. 7, compared to the N_2O route, the HNNO mechanism is most prominent in the lower temperature region of these flames—which is consistent with the higher branching ratio to HNNO relative to NH + NO at lower temperatures.

Interestingly, while the HNNO mechanism involves an additional pressure-dependent reaction beyond the N₂O mechanism, comparison of NO predictions with and without HNNO kinetics in Fig. 5 reveals that the significance of the HNNO mechanism peaks at intermediate pressures. Within this context, it is important to note that the HNNO mechanism not only has an additional pressure-dependent reaction but also involves additional reactions with radicals—such that it is higher order in radical concentration than other NO_x formation mechanisms. While the rate constants for HNNO stabilization increase with pressure, the flame simulations also indicate that the radical mole fractions decrease with pressure as pressure-dependent radical chain termination pathways suppress chain branching [49,61]. In fact, as indicated by Fig. 7, from 10 to 30 atm, the radical mole fractions decrease more than three-fold-such that radical concentrations are lower at 30 atm than at 10 atm. Furthermore, with increasing pressure, the portion of the flame where radicals reach significant mole fractions is increasingly restricted to a higher-temperature window (to overcome increased rate constants for pressure-dependent radical termination routes [49,61])—thereby suppressing reactivity in the lower temperature region where the branching ratio to HNNO from H + N₂O is comparatively higher. The reduction in both the magnitude of radical concentrations and span of radical-zone temperature windows is more pronounced for lean and stoichiometric mixtures—where HO_2 reaction with OH, the most prominent radical, is only chain terminating (to form $H_2O + O_2$ [62])—than for rich mixtures—where HO_2 reaction with H, the most prominent radical, has a chain-propagating channel to OH + OH in addition to the chain-terminating channel to $H_2 + O_2$ [51]. Correspondingly, comparison of NO predictions with and without HNNO kinetics in Fig. 5 reveals a greater influence of the HNNO mechanism at 30 atm for rich conditions than for lean conditions. (At this point, it is perhaps worth noting that the exact pressure at which the contribution of the HNNO mechanism peaks can depend on the flame temperatures—yielding higher flame temperatures—suggest the influence of the HNNO mechanism persists to higher pressures for higher flame temperatures.)

Additional analysis of the forward, backward, and net rates of $H + N_2O (+M) = t-HNNO (+M)$ reveal that the rates of HNNO consumption become sufficiently slow relative to HNNO stabilization at high pressures in lean and stoichiometric mixtures that H + N₂O = t-HNNO is in partial equilibrium-such that HNNO + radical reactions are the rate-limiting steps. Indeed, comparison of NO predictions among models with varied treatments of HNNO kinetics reveals that, for lean and stoichiometric conditions at 30 atm, predictions are only sensitive to the rate constant for the NO-forming HNNO + radical reactions (R9), (R10), (R11) and are insensitive to third-body efficiencies for HNNO stabilization and rate constants for non-NO-forming HNNO + radical reactions (e.g., (R15), (R16), (R17), (R18)). Of course, at conditions where HNNO stabilization is not a rate-limiting step (e.g., at very high pressures), the additional pressure-dependent reaction in the HNNO mechanism does not lead to a higher order pressure dependence. By contrast, at lower pressures, where $H + N_2O = t$ -HNNO is not in partial equilibrium, predictions are sensitive to rate constant parameters for formation of HNNO as well as both NO-forming and non-NO-forming consumption pathways for HNNO.

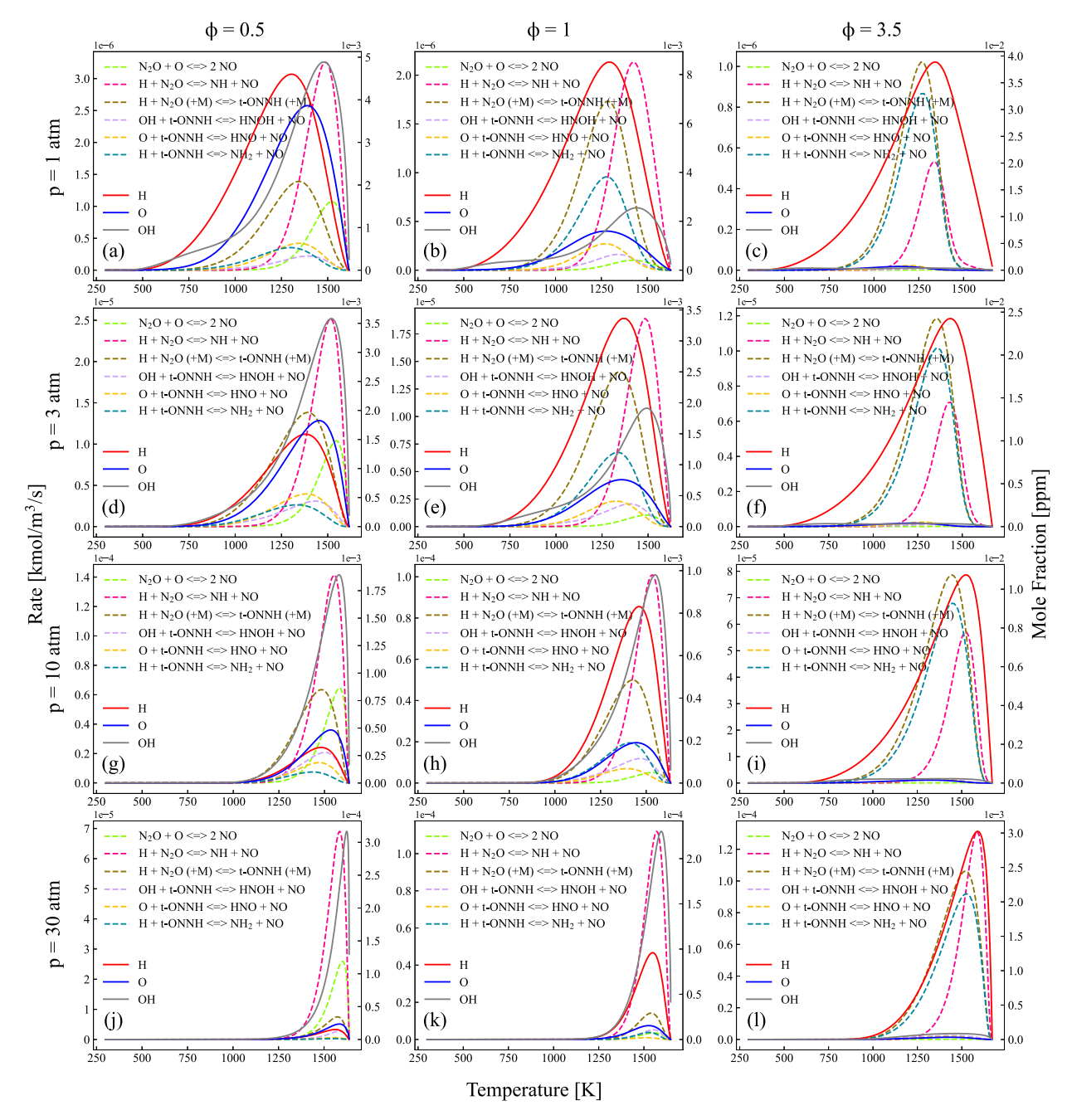


Fig. 7. Predicted mole fractions of H, OH, and O and net rates of reaction for selected reactions within the N₂O and HNNO mechanisms using the model with HNNO kinetics in the flames shown in Fig. 5.

In addition to the discussion above related to general understanding of HNNO kinetics in flames, an equally important conclusion to be drawn from Fig. 5 is that model predictions are sensitive to many aspects of the HNNO kinetic sub-model that are currently based on estimates and are subject to high uncertainties. In this regard, improved quantification of collider-specific rate constants for H + N₂O (and accompanying mixture rules [54]) and channel-specific rate constants for HNNO + radical reactions would be highly worthwhile for exact quantification of the role of HNNO in NO_x formation and quantitative predictions of NO_x in general.

5. Conclusion

Jet-stirred reactor experiments were performed for an $H_2/O_2/N_2O/NO/N_2/Ar$ reactant mixture over intermediate tem-

peratures that specifically target a new NO_x formation mechanism via an HNNO intermediate (formed from H + N_2O stabilization). In the experiments, the mole fractions of N_2O , H_2 , H_2O , and O_2 were measured using gas chromatography and the mole fractions of NO, NO_x , and NH_3 were measured using chemiluminescence with high levels of repeatability and quantified uncertainties. While model predictions using various models reproduce the qualitative behavior observed for N_2O , H_2 , H_2O , and O_2 , the experimental measurements identified appreciable amounts of NO and NH_3 at lower temperatures (~ 800 –950 K) that are not predicted by previous models. In fact, prediction uncertainties due to uncertainties in known NO_x formation pathways, other reactions, and physical model parameters were also found to be insufficient to explain the experimental observations. By contrast, model predictions with a new HNNO kinetic sub-model [13] explain the appearance of both

NO and NH_3 at temperatures near $\sim 800-950~K$ and are, in fact, in reasonable quantitative agreement with the measured mole fractions of each.

To explore the implications of the HNNO mechanism for NO_x formation from non-nitrogenous fuels in flames (a common combustion mode in many engines), freely propagating premixed flame simulations were performed using this new HNNO kinetic submodel [13] for hydrogen flames at varied pressures and equivalence ratios. These simulations reveal significant contributions from the HNNO mechanism to overall NO_x formation at all equivalence ratios. While the pressure-dependent stabilization reactions in the HNNO mechanism would lead to increased rate constants for HNNO formation at higher pressures, the flame simulations reveal that the lower radical mole concentrations in flames at higher pressures serve to reduce the rates of HNNO consumption pathways, including those that produce NO_x. Correspondingly, the significance of the HNNO mechanism is found to peak at intermediate pressures rather than increase monotonically with pressure (at least for the flame conditions explored here).

While the model predictions with HNNO kinetics and present experimental measurements are in reasonable agreement, it is of course worth noting that many aspects of this initial HNNO kinetic sub-model are currently estimated on the basis of preliminary electronic structure calculations (for HNNO + H, OH, and O) and analogy to other reactions for third-body efficiencies (for H + N₂O = HNNO) and are, likewise, subject to high uncertainties. In this regard, improved quantification of those aspects—including collider-specific rate constants for H + N₂O (and accompanying mixture rules [54]) and channel-specific rate constants for HNNO + radical reactions—would be highly worthwhile for exact quantification of the role of HNNO in NO_x formation and quantitative predictions of NO_x in general.

Declaration of Competing Interest

The authors declare that they have no known competing financial interests or personal relationships that could have appeared to influence the work reported in this paper.

Acknowledgments

The authors gratefully acknowledge support of this research by the National Science Foundation Combustion and Fire Systems program (CBET-1944004).

Supplementary material

Supplementary material associated with this article can be found, in the online version, at doi:10.1016/j.combustflame.2023. 112632.

References

- [1] J.A. Miller, C.T. Bowman, Mechanism and modeling of nitrogen chemistry in combustion, Prog. Energy Combust. Sci. 15 (1989) 287–338.
- [2] P. Glarborg, J.A. Miller, B. Ruscic, S.J. Klippenstein, Modeling nitrogen chemistry in combustion, Prog. Energy Combust. Sci. 67 (2018) 31–68.
- [3] A.C.A. Lipardi, J.M. Bergthorson, G. Bourque, NO_xemissions modeling and uncertainty from exhaust-gas-diluted flames, J. Eng. Gas Turbine Power 138 (2015) 051506.
- [4] P. Versailles, A. Durocher, G. Bourque, J.M. Bergthorson, Nitric oxide formation in lean, methane-air stagnation flames at supra-atmospheric pressures, Proc. Combust. Inst. 37 (2019) 711–718.
- [5] Y. Zeldovich, The oxidation of nitrogen in combustion and explosions, Acta Physicochim. 21 (1946) 577–628.
- [6] A. Durocher, P. Versailles, G. Bourque, J.M. Bergthorson, Impact of kinetic uncertainties on accurate prediction of NO concentrations in premixed alkane-air flames, Combust. Sci. Technol. 192 (2020) 959–985.
- [7] C.P. Fenimore, Formation of nitric oxide in premixed hydrocarbon flames, Symp. (Int.) Combust. 13 (1971) 373–380. Elsevier

- [8] L.V. Moskaleva, M.-C. Lin, The spin-conserved reaction CH+ N₂ H + NCN: a major pathway to prompt NO studied by quantum/statistical theory calculations and kinetic modeling of rate constant, Proc. Combust. Inst. 28 (2000) 2393–2401.
- [9] S.J. Klippenstein, M. Pfeifle, A.W. Jasper, P. Glarborg, Theory and modeling of relevance to prompt-NO formation at high pressure, Combust. Flame 195 (2018) 3–17.
- [10] J.W. Bozzelli, A.M. Dean, O + NNH: a possible new route for NO_x formation in flames, Int. J. Chem. Kinet. 27 (1995) 1097–1109.
- [11] A.A. Konnov, On the relative importance of different routes forming NO in hydrogen flames, Combust. Flame 134 (2003) 421–424.
- [12] M.S. Day, J.B. Bell, X. Gao, P. Glarborg, Numerical simulation of nitrogen oxide formation in lean premixed turbulent H₂/O₂/N₂ flames, Proc. Combust. Inst. 33 (2011) 1591–1599.
- [13] Q. Meng, L. Lei, J. Lee, M.P. Burke, On the role of HNNO in NO_x formation, Proc. Combust. Inst. 39 (2023) in press, doi:10.1016/j.proci.2022.08.044.
- [14] C.F. Melius, J.S. Binkley, Energetics of the reaction pathways for NH_2 + NO products and NH + NO products, Symp. (Int.) Combust. 20 (1985) 575–583.
- [15] J.W. Bozzelli, A.Y. Chang, A.M. Dean, Analysis of the reactions H + N₂O and NH + NO: pathways and rate constants over a wide range of temperature and pressure, Symp. (Int.) Combust. 25 (1994) 965–974.
- [16] S.J. Klippenstein, L.B. Harding, P. Glarborg, J.A. Miller, The role of NNH in NO formation and control, Combust. Flame 158 (2011) 774–789.
- [17] A.W. Jasper, Predicting third-body collision efficiencies for water and other polyatomic baths, Faraday Discuss. 238 (2022) 68–86.
- [18] J. Shao, R. Choudhary, A. Susa, D.F. Davidson, R.K. Hanson, Shock tube study of the rate constants for $H+O_2+M=HO_2+M$ ($M=Ar, H_2O, CO_2, N_2$) at elevated pressures, Proc. Combust. Inst. 37 (2019) 145–152.
- [19] R. Choudhary, J.J. Girard, Y. Peng, J. Shao, D.F. Davidson, R.K. Hanson, Measurement of the reaction rate of H + O₂ + M = HO₂ + M, for M = Ar, N₂, CO₂, at high temperature with a sensitive OH absorption diagnostic, Combust. Flame 203 (2019) 265–278.
- [20] J.A. Miller, S.J. Klippenstein, Theoretical considerations in the NH₂ + NO reaction, J. Phys. Chem. A 104 (2000) 2061–2069.
- [21] D.-C. Fang, L.B. Harding, S.J. Klippenstein, J.A. Miller, A direct transition state theory based analysis of the branching in NH₂ + NO, Faraday Discuss. 119 (2002) 207–222.
- [22] M.-C. Lin, Y. He, C.F. Melius, Theoretical interpretation of the kinetics and mechanisms of the HNO + HNO and HNO + 2 NO reactions with a unified model, Int. J. Chem. Kinet. 24 (1992) 489–516.
- [23] X. Han, M.L. Lavadera, A.A. Konnov, An experimental and kinetic modeling study on the laminar burning velocity of NH₃ + N₂O + air flames, Combust. Flame 228 (2021) 13–28.
- [24] K.P. Shrestha, C. Lhuillier, A.A. Barbosa, P. Brequigny, F. Contino, C. Mounaïm-Rousselle, L. Seidel, F. Mauss, An experimental and modeling study of ammonia with enriched oxygen content and ammonia/hydrogen laminar flame speed at elevated pressure and temperature, Proc. Combust. Inst. 38 (2021) 2163–2174.
- [25] Y. Zhang, O. Mathieu, E.L. Petersen, G. Bourque, H.J. Curran, Assessing the predictions of a NO_x kinetic mechanism on recent hydrogen and syngas experimental data, Combust. Flame 182 (2017) 122–141.
- [26] A. Stagni, C. Cavallotti, S. Arunthanayothin, Y. Song, O. Herbinet, F. Battin-Leclerc, T. Faravell, An experimental, theoretical and kinetic-modeling study of the gas-phase oxidation of ammonia, React. Chem. Eng. 5 (2020) 696–711.
- [27] J. Otomo, M. Koshi, T. Mitsumori, H. Iwasaki, K. Yamada, Chemical kinetic modeling of ammonia oxidation with improved reaction mechanism for ammonia/air and ammonia/hydrogen/air combustion, Int. J. Hydrog. Energy 43 (2018) 3004–3014
- [28] G.P. Smith, D.M. Golden, M. Frenklach, N.W. Moriarty, B. Eiteneer, M. Goldenberg, C.T. Bowman, R.K. Hanson, S. Song, W.C. Gardiner Jr, V. Lissianski, Z. Qin, GRI-Mech3.0.
- [29] N. Lamoureux, H.E. Merhubi, L. Pillier, S. de Persis, P. Desgroux, Modeling of NO formation in low pressure premixed flames, Combust. Flame 163 (2016) 557–575.
- [30] P. Marshall, A. Fontijn, C.F. Melius, High-temperature photochemistry and BAC-MP4 studies of the reaction between ground-state h atoms and N₂O, J. Chem. Phys. 86 (1987) 5540–5549.
- [31] R.E. Cornell, M.C. Barbet, M.P. Burke, Toward a more comprehensive understanding of the kinetics of a common biomass-derived impurity: NH₃ oxidation by N₂O in a jet-stirred reactor, Energy Fuels 35 (2021) 13338–13348.
- [32] R.E. Cornell, M.C. Barbet, J. Lee, M.P. Burke, NH₃ oxidation by NO₂ in a jet-stirred reactor: the effect of significant uncertainties in H₂NO kinetics, Appl. Energy Combust. Sci. 12 (2022) 100095.
- [33] M.C. Barbet, R.E. Cornell, M.P. Burke in preparation.
- [34] M.P. Burke, Harnessing the combined power of theoretical and experimental data through multiscale informatics, Int. J. Chem. Kinet. 48 (2016) 212–235.
- [35] O. Herbinet, P.M. Marquaire, F. Battin-Leclerc, R. Fournet, Thermal decomposition of n-dodecane: experiments and kinetic modeling, J. Anal. Appl. Pyrolysis 78 (2007) 419–429.
- [36] O. Herbinet, B. Husson, Z. Serinyel, M. Cord, V. Warth, R. Fournet, P.-A. Glaude, B. Sirjean, F. Battin-Leclerc, Z. Wang, M. Xie, Z. Cheng, F. Qi, Experimental and modeling investigation of the low-temperature oxidation of n-heptane, Combust. Flame (2012) 3455–3471.
- [37] D. Matras, J. Villermaux, Un éacteur continu parfaitement agité par jets gazeux pour l'étude cinétique de réactions chimiques rapides, Chem. Eng. Sci. 28 (1973) 129–137.

- [38] R. David, D. Matras, Règies de construction et d'extrapolation des réacteurs auto-agités par jets gazeux, Can. J. Chem. Eng. 53 (1975) 297–300.
- [39] W.W. Ayass, Mixing in Jet-Stirred Reactors with Different Geometries, 2013 Ph.D. thesis.
- [40] W.W. Ayass, E.F. Nasir, A. Farooq, S.M. Sarathy, Mixing-structure relationship in jet-stirred reactors, Chem. Eng. Res. Des. 111 (2016) 461–464.
 [41] O. Herbinet, F. Battin-Leclerc, Progress in understanding low-temperature or-
- [41] O. Herbinet, F. Battin-Leclerc, Progress in understanding low-temperature organic compound oxidation using a jet-stirred reactor, Int. J. Chem. Kinet. 46 (2014) 619–639.
- [42] L. Marrodán, Y. Song, M. Lubrano Lavadera, O. Herbinet, M. De Joannon, Y. Ju, M.U. Alzueta, F. Battin-Leclerc, Effects of bath gas and NO_x addition on n-pentane low-temperature oxidation in a jet-stirred reactor, Energy Fuels 33 (2019) 5655–5663.
- [43] P. Azay, G.-M. Côme, Temperature gradients in a continuous flow stirred tank reactor, Ind. Eng. Chem. Process. Des. Dev. 18 (1979) 754–756.
- [44] S. Salimian, R.K. Hanson, C.H. Kruger, Ammonia oxidation in shock-heated NH₃-N₂O-Ar mixtures, Combust. Flame 56 (1984) 83–95.
- [45] K. Kohse-Höinghaus, D.F. Davidson, A.Y. Chang, R.K. Hanson, Quantitative NH₂ concentration determination in shock tube laser-absorption experiments, J. Quant. Spectrosc. Radiat. Transf. 42 (1989) 1–17.
- [46] O. Mathieu, E.L. Petersen, Experimental and modeling study on the high-temperature oxidation of ammonia and related NO_x chemistry, Combust. Flame 162 (2015) 554–570.
- [47] D.G. Goodwin, H.K. Moffat, R.L. Speth, Cantera: an object-oriented software toolkit for chemical kinetics, thermodynamics, and transport processes, 2018. Version 2.4.0.
- [48] S.J. Klippenstein, L.B. Harding, P. Glarborg, Y. Gao, H. Hu, P. Marshall, Rate constant and branching fraction for the NH₂ + NO₂ reaction, J. Phys. Chem. A 117 (2013) 9011–9022.
- [49] M.P. Burke, M. Chaos, F.L. Dryer, Y. Ju, Negative pressure dependence of mass burning rates of H₂/CO/O₂/diluent flames at low flame temperatures, Combust. Flame 157 (2010) 618–631.
- [50] M.C. Barbet, M.P. Burke, Impact of "missing" third-body efficiencies on kinetic model predictions of combustion properties, Proc. Combust. Inst. 38 (2021) 425–432.

- [51] M.P. Burke, M. Chaos, Y. Ju, F.L. Dryer, S.J. Klippenstein, Comprehensive H₂/O₂ kinetic model for high-pressure combustion, Int. J. Chem. Kinet. 44 (2012) 444–474
- [52] M.P. Burke, R. Song, Evaluating mixture rules for multi-component pressure dependence: H + O₂ (+M) = HO₂ (+M), Proc. Combust. Inst. 36 (2017) 245–253.
- [53] L. Lei, M.P. Burke, Evaluating mixture rules and combustion implications for multi-component pressure dependence of allyl + HO₂ reactions, Proc. Combust. Inst. 37 (2019) 355–362.
- [54] L. Lei, M.P. Burke, Bath gas mixture effects on multichannel reactions: insights and representations for systems beyond single-channel reactions, J. Phys. Chem. A 123 (2018) 631–649.
- [55] L. Lei, M.P. Burke, Mixture rules and falloff are now major uncertainties in experimentally derived rate parameters for $H + O_2 (+ M) = HO_2 (+ M)$, Combust. Flame 213 (2020) 467–474.
- [56] L. Lei, M.P. Burke, Dynamically evaluating mixture effects on multi-channel reactions in flames: a case study for the CH₃ + OH reaction, Proc. Combust. Inst. 38 (2021) 433–440.
- [57] C.E. LaGrotta, M.C. Barbet, L. Lei, M.P. Burke, Towards a high-accuracy kinetic database informed by theoretical and experimental data: CH₃ + HO₂ as a case study, Proc. Combust. Inst. 38 (2021) 1043–1051.
- [58] C.E. LaGrotta, Q. Meng, L. Lei, M.C. Barbet, Z. Hong, M.P. Burke, Resolving discrepancies between state-of-the-art theory and experiment for HO₂ + HO₂ via multiscale informatics, J. Phys. Chem. A 127 (2023) 799–816.
- [59] C.E. LaGrotta, M.C. Barbet, L. Lei, M.P. Burke, MSI: A package for MultiScale Informatics, https://github.com/TheBurkeLab/MSI.
- [60] A. Durocher, G. Bourque, J.M. Bergthorson, Quantifying the effect of kinetic uncertainties on NO predictions at engine-relevant pressures in premixed methane-air flames, J. Eng. Gas Turbine Power 142 (2020) 061008.
- [61] M.P. Burke, F.L. Dryer, Y. Ju, Assessment of kinetic modeling for lean H₂/CH₄/O₂/diluent flames at high pressures, Proc. Combust. Inst. 33 (2011) 905–912.
- [62] M.P. Burke, S.J. Klippenstein, L.B. Harding, A quantitative explanation for the apparent anomalous temperature dependence of OH + $\rm HO_2 = H_2O + O_2$ through multi-scale modeling, Proc. Combust. Inst. 34 (2013) 547–555.